ISSN (Online) 2456-1290
International Journal of Engineering Research in Mechanical and Civil Engineering (IJERMCE)
Vol 2, Issue 4, April 2017

Review of process, material and properties of spot welding for automotive bodies

[1] Prof.Sushil T Ambadkar, [2] Dr.DeepakV.Bhope,
[1] Asst Professor,Department of Mechanical Engineering, [2] Professor, Department of Mechanical Engg
[1] Government College of Engineering,Chandrapur,
[2] Rajiv Gandhi College of Engineering,Research and Technology,Chandrapur

Abstract: **-- Resistance spot welding has been widely used as welding process for manufacturing auto-body, aerospace and electronics structures. The motor vehicle makes extensive application of Resistance spot welding with 2000 and 5000 spot welds. The process is used in these applications due to high productivity, flexibility, and suitability. It is the mechanical performance of spot weld which controls performance of vehicle structure in crash.**

In this review , type of the joints covered are i) Spot welding of triple-thin-sheet aluminium alloy ii)Resistance spot welding of three different dissimilar aluminium alloy stackups that included die cast Aural2T7 to Aural2T7,Aural2T7 to AA5754O, and Aural2T7 to AA6022T4 iii) Resistance spot welding between AISI 430 ferritic stainless steel and drawing quality special killed (DQSK) low-carbon steel iv) Resistance spot welding of AZ31B Mg alloy to Al Alloy 5754 using Zn foil and Zn-coated steel interlayer v) Spot welding of advanced high strength steels

The materials considered are Aluminium, Aural2T7, AA5754O and AA6022T4, AISI 430 ferritic stainless steel and drawing quality special killed (DQSK) low-carbon steel, AZ31B Mg alloy and Al Alloy 5754.The failure modes, changes obtained in microstructure, bonding, phases and properties for different materials welded using spot welding are discussed.

In spot welding of triple-thin-sheet aluminium alloy, an analytical model, which is suitable for the three-sheet aluminium alloy resistance spot weld, was proposed to ensure the pullout failure mode. The critical weld button size required to ensure the pullout failure mode was obtained. Weld nuggets produced with spot welding of die cast Aural2T7 to Aural2T7,Aural2T7 to AA5754O, and Aural2T7 to AA6022T4 were compared for yield strength, strengthening etc.

The microstructure and mechanical performance of dissimilar resistance spot welds between AISI 430 ferritic stainless steel and drawing quality special killed (DQSK) low-carbon steel was discussed with reference to peak load, failure energy, and failure mode during the tensile-shear test. Resistance spot welding of AZ31B Mg alloy to Al Alloy 5754 was studied using Zn foil and Zn-coated steel inter-layers. Mechanical properties and microstructure of the welds were analyzed.

In spot welding of advanced high strength steels an optimization strategy for the spot welding process was developed to improve fatigue performance of spot welds.

Keywords**- Resistance spot welding, material, failure mode, mechanical behaviour**

INTRODUCTION

Resistance spot welding is commonly used in both automotive and aerospace industries. Resistance spot welding is a process in which a small weld is formed between two metal work pieces through localized melting due to resistance heating caused by a passage of electric current. Because of the simplicity of the process, it is easily automated, and once the welding parameters are set, repeatable welds are possible.

JOINTS UNDER CONSIDERATION

Y. Li, Y. Zhang, Z. Luo, H. Shan, Y. Q. Feng, And Z. X. Ling [1] in their study used, 6061-T6 aluminum alloy sheets with thicknesses of 1, 1.5, and 2.0 mm. Two thickness combinations were used in the experiments. From the upper electrode tip to the lower one, the two

ISSN (Online) 2456-1290
International Journal of Engineering Research in Mechanical and Civil Engineering (IJERMCE)
Vol 2, Issue 4, April 2017

thickness combinations were 1.0/1.0/1.0 mm and 1.5/1.0/2.0 mm, respectively.

J. Kang, B. Shalchi-Amirkhiz, Y. Chen, D. R. Sigler, And B. E. Carlson [2] used 3-mm-thick Aural-2-T7 (AlSi10Mg-T7) high pressure die cast sheets, 2-mm-thick AA5754-O (Al-Mg3 solid-solution hardened alloy), and AA6022-T4 (Al-Si-Mg precipitation-hardened alloy) wrought alloy rolled sheets for welding. General Motors's proprietary MRD resistance spot welding process was used to weld three types of aluminum dissimilar spot welds, namely, Aural- 2-T7 to Aural-2- T7, Aural-2-T7 to AA5754-O, and Aural- 2-T7 to AA6022-T4. Weld coupons were 150 mm long and 38 mm wide as shown in fig 2.

M. Pouranvari, S. P. H. Marashi, And M. Alizadeh-Sh [3] used AISI 430 ferritic stainless steels and DQSK AISI 1004 low-carbon steel as base metals. The thickness of lap welded sheets was 1.5 mm and length 140 mm .

P. Penner, l. Liu, a. Gerlich, and y. Zhou [4] used sheets of mg alloy az31b-h24 and al alloy 5754-o,dimensions of welding coupons being 100× 35 × 2 mm. Commercially pure zn foil with thickness of 0.25 mm and hot-dip galvanized Hsla steel with thickness of 0.7 mm were used as interlayer in this study. 1.6-mm galvannealed trip590 and 1.6-mm hot dip galvanized (hdg) dp600 were chosen by s. K. Vanimisetti and d. R. Sigle [5]. The conventional multipulse weld schedule for 1.6-mm ahss was used. Weld force used was 4.2 kn with weld current of 7 to 11 ka. Electrodes were made of cu-zn, c15000 alloy with 4.8-mm face diameter.

MATERIALS

The nominal chemical compositions of the materials considered in this review are given in table 1.

S N	Base Metal	Composition Wt %	Weld type	Weld details	Ref
1	6061T6 Aluminum Alloy	Si-0.56 Mg-1.10 Zn-0.25 Cu-0.25 Mn-0.15 Fe-0.70 Cr-0.18 Ti-0.15 Al- Balance	Spot weld	Two stack-ups, 1.0/1.0/1.0 mm and 1.5/1.0/2.0 mm, triple-thin-sheet	1
2	Aural2T7 AA5754O AA6022T4	Ti ≤0.15 Si-1-11.5 Mn- 0.3–0.6 Fe- ≤ 0.30 Mg-0.1–3.6 Sr-0.01–0.018 Cu≤ 0.25 Cr≤ 0.30 Zn≤ 0.20 Al-bal	Spot weld	Three different dissimilar aluminum alloy stack-ups, Aural2T7 to Aural2T7, Aural2T7 to AA5754O, and Aural2T7 to AA6022T 4	2
3	a)AISI430 FSS, b)DQSK Low-Carbon Steel	a)AISI430 C -0.024,Mn-b)0.513,Cr -17.002,Si-0.383,Ni-0.066,Mo-0.026 DQSK-C -0.044 Cr-0.010,Ni-0.031,Mn-0.202,Si-0.001,S-0.03,Mo-0.003	Spot weld	Lap joint of AISI 430 FSS to DQSK low-carbon steel	3
4	a)Mg alloy AZ31B-H24 b)Al Alloy 5754-O,	a)Al-2.5,Zn-1,Mn-0.2,Si-0.1, Mg-Bal b) Mn-0.25,Fe-0.2,Mg-3, Si-0.2, Al-bal	Spot weld	AZ31B Mg alloy to Al Alloy 5754 , Zn foil and Zn coated steel interlayer.	4
5	a) Galvanneal ed TRIP590 Steel, b)hot dip galvanized DP600	a) C-0.175,Mn-2, Si and Al-2 b) C-0.15,Mn-2.2, Si and Al-2.5	Spot weld	Lap shear configurati on,1.6 mm thin	5

ISSN (Online) 2456-1290
International Journal of Engineering Research in Mechanical and Civil Engineering (IJERMCE)
Vol 2, Issue 4, April 2017

SPOT WELDING OF TRIPLE-THIN-SHEET ALUMINIUM ALLOY

Y. Li, Y. Zhang, Z. Luo, H. Shan, Y. Q. Feng, And Z. X. Ling [1] investigated failure mechanism of three-sheet 6061-T6 aluminum alloy resistance spot welds, especially the failure mode transition behavior of the spot welds. Four types of joints were designed and the mechanical properties of three-sheet RSWs are also investigated. The joint specification of test specimen is shown in fig 1.

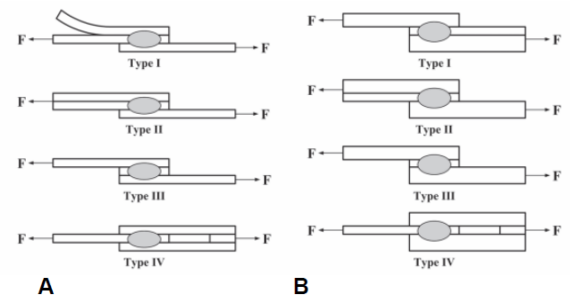

Fig. 1 — joint designs of the three sheet aa6061t6 welds: a — 1.0/1.0/1.0 mm stack; b — 1.5/1.0/2.0 mm stack.

In the Type I and II joints, only one interface bore the tensile force during the test. In the Type III and IV joints, both of the two interfaces bore the tensile force during the test. Spot welding was performed using a 220-kW direct current (DC) inverter RSW machine.

The tensile-shear tests were performed at a crosshead of 1 mm /min with a CSS-44100 material test system. The maximum load of the CSS-44100 material test system is 200 kN and the initial distance between the crosshead was 125 mm (the gripped zone on each sheet was 25 mm). The peak load was evaluated using the average value of the three complete tensile-shear tests. The "button size" was used to evaluate the weld quality rather than the "nugget size" (Ref. 6). Step-by-step tensile-shear tests were used to investigate the failure processes of the weld joints. Seven specimens were obtained from different stages (load raising stage, peak load stage, load drop stage, and final fracture stage) during the tensile-shear test. The seven specimens were ground, polished, and etched using standard metallographic procedures. The cross sections of the welds were etched by Keller's reagent The Vickers micro-3 hardness test was performed using an indenter load of 100 g for a period of 10 s.

Microstructure

From nugget edge to nugget center, the microstructure is partially melted zone (PMZ), columnar grain zone (CGZ), and equiaxed grain zone (EGZ). The columnar grain has two morphologies, the columnar grain with large secondary dendrite arm spacing (LCGZ) and the columnar grain with small secondary dendrite arm spacing (SCGZ).The authors found that the LCGZ was easier to form at the lower interface (close to the negative electrode) because of the Peltier effect (Refs. 07,08).The lowest micro-hardness appears in the LCGZ, which has a coarser structure and less alloy content.

Failure Mode Transition in Types I and II (Equal Thickness Stacks)

Three types of failure modes, interfacial (IF) failure, partial thickness, partial pullout (PT-PP) failure (Ref. 09), and pullout (PO) failure were observed in joint Types I and II, as shown in Fig. 3.

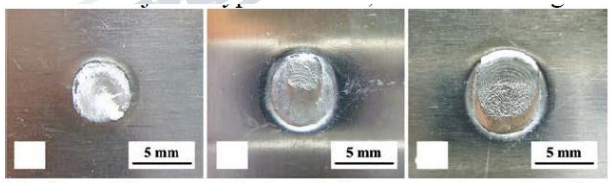

fig.2— photos of the failure surface in the 1.0/1.0/1.0 mm stack: interfacial failure; partial thickness-partial pullout failure; pull-out failure.

The load-displacement curves indicated similarity of the mechanical behavior of the type i and ii joints, as shown in fig. 3.

ISSN (Online) 2456-1290
International Journal of Engineering Research in Mechanical and Civil Engineering (IJERMCE)
Vol 2, Issue 4, April 2017

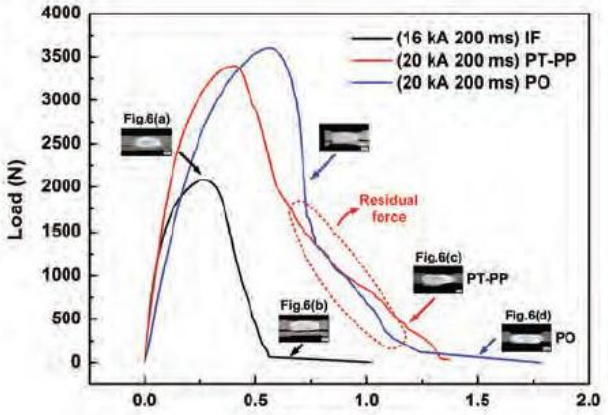

fig. 3 — typical load-displacement curves of the type i and ii joint in the 1.0/1.0/1.0 mm stack.

Figure 4 shows the effect of button size on the peak load and energy absorption of joint designs i and ii. Simple linear regression was applied to both the data obtained from joints i and ii, and a best fit line with a coefficient of determination (r2) of 0.878, was obtained. The relatively high value of r2 suggested that a linear relationship exists between the peak load and button size. This phenomenon is also observed by han et al. (ref. 10) and sun et al. (ref. 11).

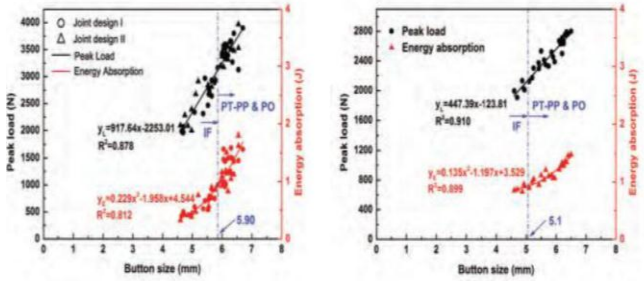

Fig. 4 — effect of button size on the peak load and energy of joint designs i and ii in the 1.0/1.0/1.0 mm stack. 5 - effect of button size on the peak load and energy absorption of the type iii joint in the 1.0/1.0/1.0 mm stack.

Failure of Joint Type III and IV

IF,PT-PP, and PO failures observed in the Type III joint were similar to joint Types I and II and analysis of the PO failure mode was discussed as it was found to be different from the previous case. The crack began to form at LCGZ and propagated through the SCGZ and LCGZ interface. A crack was also found on the other workpiece/workpiece interface indicating competition between the two interfaces in a three-sheet spot weld joint, and that failure will occur on the weaker one. It was verified that the LCGZ is the weak area in a spot weld. The PO mode, also indicated competition between the two interfaces for crack during the tensile-shear test.

Figure 5 shows the effect of button size on the peak load and energy absorption of joint design III. The minimum button size that guarantees a PO mode was 5.1 mm. The results are similar to the case of joint Types I and II.The failure modes of type IV joint were different from those of joint Types I,II, and III due to pure shear. When the nugget size was small, both of the two interfaces failed through double interfacial failure (DIF). When the nugget size grew larger, joint showed one interfacial/ one pullout (IF/PO) failure. When the nugget size was large enough, the base metal fractured through base metal fracture (BMF) failure.

Figure 6 shows the load-displacement curve and microstructures of the Type IV weld joint that failed in the BMF mode. The curve has a “platform,” which indicates that the crack is propagating in the base metal and, therefore, the load is relatively stable. The weld nugget had very small deformation during the tensile process compared with those that failed in the DIF and IF/PO modes. This indicates that the weld nugget was large enough to resist being squeezed.

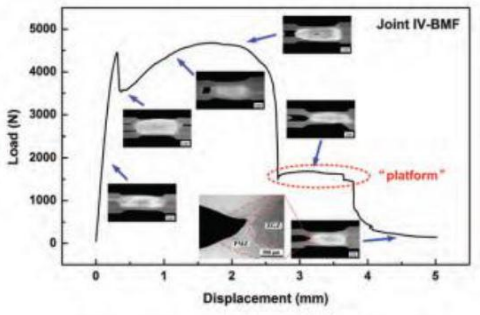

ISSN (Online) 2456-1290
International Journal of Engineering Research in Mechanical and Civil Engineering (IJERMCE)
Vol 2, Issue 4, April 2017

Fig. 6 — typical load-displacement curve of type iv weld joints in the 1.0/1.0/1.0 mm stack that failed in bmf mode (22 ka, 200 ms).

CHARACTERIZATION OF DISSIMILAR ALUMINUM ALLOY RESISTANCE SPOT WELDS

J. Kang, B. Shalchi-Amirkhiz, Y. Chen, D. R. Sigler, And B. E. Carlson [2] used automotive body materials 3-mm-thick Aural-2-T7 (AlSi10Mg-T7) high pressure die cast sheets, 2- mm-thick,AA5754-O (Al-Mg3 solid-solution hardened alloy), and AA6022-T4 (Al-Si-Mg precipitation-hardened alloy) wrought alloy rolled sheets.

Spot welding was done using a medium-frequency DC (MFDC) weld control and transformer. The MRD electrode was made from C15000 copper alloy and has a 12-mm face diameter with a 25-mm radius of curvature and 5 upstanding rings. The Force was 4.9-6.7 kN, Preheat Time 30-50 ms, Cool Time 10 ms, Weld Time 156-267 ms, Weld Current 27-33.5 kA in spot welding schedules. Some of the aluminum spot welds underwent "baking" i.e., e-coat employed within the assembly plant paint shop, i.e., a thermal cycle of 30 min in total at 177$_0$C. These were "baked samples," whereas those not subjected to the bake simulation were denoted as "as-welded samples."

Some of the spot weld specimens were sectioned through the cross section perpendicular to the length direction and mounted for micro-hardness measurements and macrostructure observations following standard metallographic procedures. Shear specimens (Fig.7) were made with the shear zone located at the center of the weld nugget for weld nugget shear test specimens, or 6 mm away from the center of the weld nugget for HAZ shear test specimens.

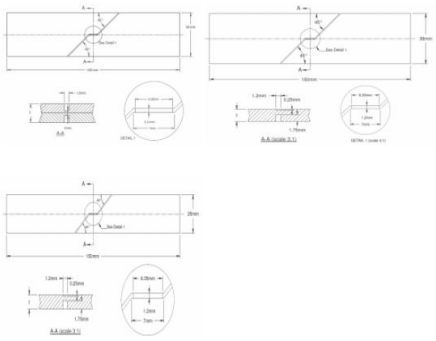

fig. 7 — shear specimen design for the following: aural2t7 to aural2t7and aural2t7to aa5754o spot welds; aural2t7 to aa6022t4 spot welds where the aa6022t4 side was removed; haz at the aural2t7 or aa6022t4 side where the other pieces were removed.

Macrostructures and micro-hardness analysis

From Figs. 8-10, macrostructures shows much greater penetration into the Aural-2-T7 side of the stack-up in both the Aural-2-T7 to AA5754-O welds and Aural-2-T7 to AA6022-T4 welds. Figure 10 exhibits the unusual microstructure formed with very little penetration into the AA6022-T4 side for the Aural-2-T7 to AA6022-T4 spot welds.

The weld nugget size was easily revealed during peel testing. Fig. 9 showed the diameter of the weld nugget is noticeably smaller at the AA5754-O side (e.g., 6.5 mm) than the Aural-2-T7 side (e.g., 8.0 mm). Figs. 8–10 showed that all the weld nuggets have significantly higher micro-hardness than the base alloy sheet. In addition, for the baked welds shown in Figs. 9 and 10 the thermal cycle does not impact the hardness of the weld nuggets.

However, in the Aural-2-T7 to AA6022-T4 spot welds shown in Fig. 10, an increase of 10 Hv is observed after the e-coat at a spot 6 mm away from the center of the weld nugget. This was the area of interest chosen for the shear test of the HAZ.

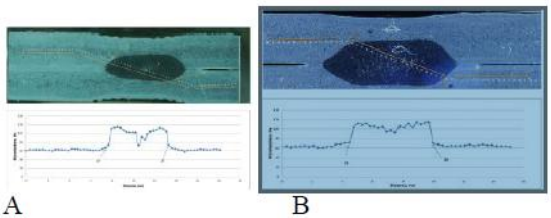

A B

Fig. 8 — Macrostructure and microhardness of Aural2T7 to Aural2T7 spot weld: A — As welded sample for welding schedule 1; B — as welded sample for welding schedule 2.

ISSN (Online) 2456-1290
International Journal of Engineering Research in Mechanical and Civil Engineering (IJERMCE)
Vol 2, Issue 4, April 2017

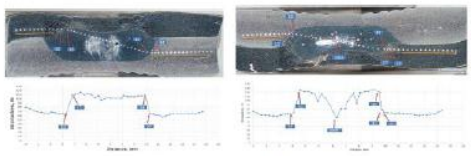

A B

Fig. 9 — Macrostructure and microhardness of Aural2T7 to AA5754O spot weld: A — As welded sample; B — baked sample.

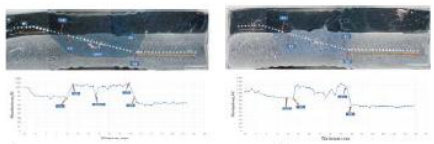

A B

Fig. 10 — Macrostructure and microhardness of Aural2T7 to AA6022 spot weld: A — As welded sample; B — baked sample.

Based on the shear angle maps at maximum load For the weld nuggets and haz in the as-welded Condition measurements, the shear strains over the Shear zone were calculated and converted to Effective strains.these illustrate that the tensile Strength of all three weld nuggets (triangular data) Are higher than the base metal substrate.tensile Stress-strain curves for the haz for all three stack5 Up combinations, the measured tensile stress-strain Curves in the aural-2-t7 haz were slightly lower Compared to that of aural-2-t7 base metal Regardless of testing conditions, i.e., whether aswelded Or baked. This means the haz in the Aural-2-t7 side was indeed insensitive to the paint Bake simulation.there was a significant increase in Yield strength of the haz in aa6022-t4 compared To the base metal substrate, but a corresponding

Decrease in work hardening of the haz compared To the base material. After the paint bake cycle, an Appreciable increase in yield strength was observed Due to age hardening as the bake temperature of 1770c is close to the solution aging temperature of 1800c for aa6022-t4 (refs. 10, 11). The microhardness measurements in the current

Work for the aa5754-o in as-welded and as-baked Conditions indicate no haz, although Metallographic analysis of aa5754 welds by Zhang and senkara does indicate a region adjacent To the weld having darkened and widened grain Boundaries indicative of a haz (ref. 12).

The fib images of the microstructure near the Faying interface of the aural-2-t7 and weld nugget For all three spot welds showed the primary Aluminum grains and pure si for all three weld Nuggets to be much finer compared to the die cast Aural-2-t7 base metal where typical spheroidized And isolated globules of si were present, indicating The addition of sr as a modifier in its chemistry (ref. 13).

WELDING OF DISSIMILAR AISI 430/DQSK STEELS RESISTANCE SPOT WELDS

M. Pouranvari, S. P. H. Marashi, And M. Alizadeh-Sh investigated the welding metallurgy of dissimilar RSW of ferritic stainless steel and DQSK low-carbon steel as base metals sheets with. thickness of 1.5 mm.

Figure 11A shows the tensile-shear sample dimensions. Failure modes were determined from the failed samples. Peak load (measured as the peak point in the load-displacement curve) and failure energy (measured as the area under the load displacement curve up to the peak load) were extracted from the load displacement curve — Fig. 11B. The amount of failure energy was calculated by measuring the area under the load-displacement curve up to the peak load. Microstructure characterization of the weldment was conducted by performing standard metallography procedure.The FZ size was measured on the metallographic cross sections at the low-carbon steel side. A Vickers microhardness test was performed to obtain a diagonal hardness profile using an indenter load of 10 g.

ISSN (Online) 2456-1290
International Journal of Engineering Research in Mechanical and Civil Engineering (IJERMCE)
Vol 2, Issue 4, April 2017

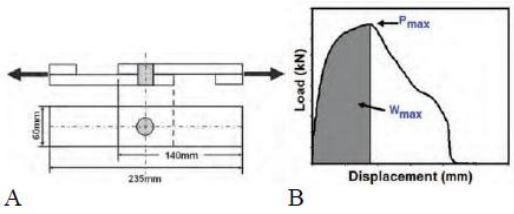

Fig. 11— A — The tensile-shear specimen dimensions; B — a typical load-displacement curve along with the extracted parameters. P_{max}: Peak load, W_{max}: Energy absorption.

METALLURGICAL CHARACTERISTICS OF HAZ OF AISI 430 STEEL

The microstructure of the aisi 430 base metal indicated a fully ferritic microstructure along with evenly distributed carbides. In the haz, microstructure is influenced by phase transformations induced by the welding thermal cycle. According to the temperature distribution, the haz was divided into two distinct metallurgical transformation zones, namely high-temperature haz (hthaz) and low-temperature haz (lthaz). The phase transformations in these zones are detailed as follows:

1) HTHAZ - based on the pseudo-binary diagram, in this region, bm microstructure transforms to fully □ -ferrite microstructure at the elevated temperature. The carbide precipitates in the bm are completely dissolved. Upon cooling, a ferritic microstructure is retained and some reprecipitation of the carbides occurred.

2) LTHAZ. Based on the pseudo-binary diagram in this region, the BM microstructure transforms to ferrite plus austenite at the elevated temperature. The amount of austenite at the grain boundaries of ferrite strongly depends on the carbon content of the alloys. Due to the low carbon content of the investigated AISI 430 steel (i.e., 0.024 wt-%), a very limited amount of austenite is formed in the LTHAZ. The high-temperature austenite is transformed to martensite during cooling.

HAZ OF DQSK STEEL

HAZ microstructure of the DQSK steel side is more heterogeneous than that of the FSS side due to martensitic and eutectoid transformations. According to the temperature distribution, the HAZ of the DQSK steel side can be divided into two distinct metallurgical transformation zones, including upper-critical HAZ and inter-critical HAZ. The phase transformations in these zones are detailed as follows:

1) Upper-Critical HAZ (UCHAZ). This region experiencing peak temperatures above Ac3,can be divided into the following zones: coarse-grained HAZ (CGHAZ)and fine-grained HAZ (FGHAZ). In CGHAZ, which is adjacent to the FZ, both the high cooling rate and large austenite grain size coupled with the formation of the carbon-rich austenite promote the formation of the martensite (Ref. 14)

2) Inter-Critical HAZ (ICHAZ). In the case of DQSK steel, the microstructure consists of fine ferrite grains and pearlite, which pearlite amount decreases as it gets closer to BM . The volume fraction of pearlite in the ICHAZ is higher than that of in the BM due to reaustenization in the ICHAZ. Decreasing peak temperature in the intercritical region (i.e., by moving away the FZ line) results in lower pearlite volume fraction. The ICHAZ is evidenced by fuzzy pearlite

Fusion Zone

Figure 12A and B shows the microstructure with volume fraction of ferrite and martensite as calculated 28 and 72%, respectively. For FSS/DQSK welds, the melting ratio is considered as 60/40. Therefore, the FZ chemical composition of FSS/DQSK welds is

Fe-10.2,Cr-0.03C-0.038 Mn- 0.23Si-0.04Ni-0.01.

Considering the low carbon content of the FZ, the Fe-Cr binary phase diagram was used as a reference to track phase transformations in the FZ of the FSS/DQSK weld. Under the non-equilibrium cooling condition, the formed austenite was transformed to martensite. Regarding the

ISSN (Online) 2456-1290
International Journal of Engineering Research in Mechanical and Civil Engineering (IJERMCE)
Vol 2, Issue 4, April 2017

transformation of austenite to martensite in the FZ, three points were considered.

1) Austenite Stability - Self et al.(Ref. 15) in their work on the austenite stability obtained an expression for the martensite start temperature (Ms) as a function of alloy composition. Their equation is given as follows:

Ms = 526 – 12.5 Cr – 17.4 Ni – 29.7 Mn – 31.7 Si

– 354 C – 20.8 Mo – 1.34 (CrNi) + 22.41 (Cr+Mo)C

For FSS/DQSK welds, the Ms was calculated as 3900C indicating that the austenite is not stable at room temperature, and it transforms to martensite, as was observed.

2) Volume Fraction of Martensite. The volume fraction of martensite in the FZ depends on the volume fraction of austenite present in the weld nugget at high temperatures, which is controlled by Ferrite to Austenite phase transformation.. Upon a rapid cooling process (e. g., welding), the transformation Ferrite to Austenite has less time to occur.The phase transformation sequence in the FZ of dissimilar FSS/DQSK welds under rapid cooling of RSW showed martensite and

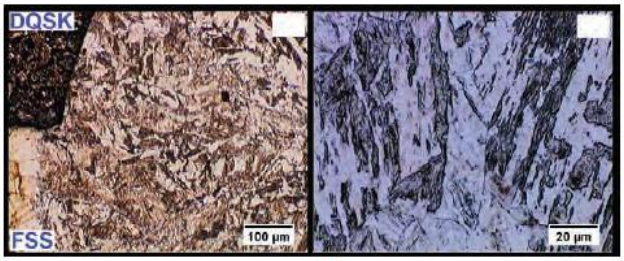

A B

Fig. 12 — A and B — Fusion zone microstructure of FSS/DQSK dissimilar resistance spot weld.

3) FZ Microstructure Prediction Using Conventional Constitution Diagrams.

It has been proved that the conventional constitution diagrams (e. g., Schaeffler diagram and Balmforth and Lippold) can be used to predict the FZ microstructure of arc welds of joints involving stainless steels.Since the cooling rate in RSW is much higher than the arc welding, a higher volume fraction retained Ferrite is formed in the FZ of the weld made using RSW. Therefore, the presence of a high-volume fraction of Ferrite can be attributed to the rapid cooling rate of RSW, which suppresses the completion of post-solidification transformation of ferrite to austenite.

Hardness Characteristics.

Figure 13 shows a typical hardness profile of FSS/DQSK welds.The hardness of the HAZ in the DQSK is higher than that of the ferritic base metal due to the formation of martensite and pearlite in these regions, respectively. The hardness of the HAZ in FSS was higher than that of the AISI 430 base metal. The higher hardness of the HTHAZ compared to the BM was due to the precipitation of carbides. The higher hardness of the LTHAZ compared to the HTHAZ was due to martensite formation in ferrite grain boundaries and its finer grain size. The hardness of the FZ is higher than both that of the base metals and HAZs, which can be attributed to the martensite formation in the FZ.

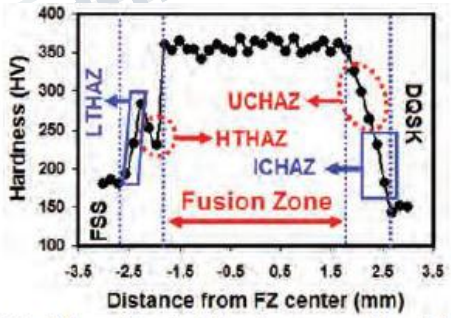

Fig. 13 — Typical hardness profile of dissimilar AISI 430/DQSK resistance spot welds.

ISSN (Online) 2456-1290
International Journal of Engineering Research in Mechanical and Civil Engineering (IJERMCE)
Vol 2, Issue 4, April 2017

Failure Mode

Both interfacial failure (IF) and double pullout failure (DPF) modes were observed during the tensile-shear testing of the FSS/DQSK welds. The increase in welding current ,not only indicated the enlargement of the weld nugget, but the failure mode was changed from IF to DPF. To avoid IF mode, a minimum welding current of 7 kA and minimum FZ size of 4.18 mm should be used for welding of the FSS/DQSK joint.

Mechanical Properties

To explore the mechanical properties of the spot welds, peak load and energy absorption were measured. Figure 14A indicated that the welding current has a significant effect on the load carrying capacity and energy absorption capability of the spot welds under the tensile-shear static test. Load carrying capacity and energy absorption capability of spot welds depend on their physical attributes, especially weld nugget size, failure mode, and failure location strength. According to Fig. 14B, the weld nugget size significantly affects the loaddisplacement characteristics of dissimilar FSS/DQSK welds. To examine the relationship between the peak load and failure energy and weld nugget size, a scatter plot of peak load (and failure energy) vs. weld size was constructed. Since the weld nugget has a asymmetrical shape, the FZ size at sheet/sheet interface in the DQSK steel, which is smaller than that of the FSS side, was measured.

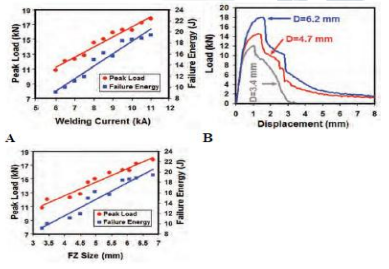

Fig. 14 — A — Effect of FZ size D on the load-displacement characteristics during the tensile-shear testing; B — welding current vs. peak load and energy absorption; C — fusion zone size vs. peak load and energy absorption of dissimilar AISI 430/DQSK resistance spot welds.

RESISTANCE SPOT WELDING OF ALUMINUM TO MAGNESIUM WITH ZNCOATED STEEL INTERLAYERS

P. Penner, L. Liu, A. Gerlich, And Y. Zhou (4), used welding specimens of Mg alloy AZ31B-H24 and Al Alloy 5754-O and pure Zn foil with thickness of 0.25 mm and hot-dip galvanized HSLA steel with thickness of 0.7 mm were used as interlayers. Metallographic weld coupons and the fracture surface of the samples were analyzed using optical and scanning electronmicroscopy (SEM). Nugget sizes of welds were measured from cross sections, with three measurements for each welding condition. Vickers micro-hardness test was performed along the diagonal across the weld. Each indentation was made with a 100-g load and 15-s indentation time, with the distance between each indentation equal to 0.25 mm.

Mechanical Properties

The use of a 0.25-mm-thick pure Zn foil interlayer was first attempted with welding currents of 16 to 32 kA, Joint strengths could not meet the requirements of AWS D17.2, Specification of Resistance Welding for Aerospace Applications, may be due to extensive intermetallic formation occurred in the nugget. Since poor quality welds were produced with a Zn-foil interlayer due to mixing of Al, Mg, and Zn, a Zncoated steel interlayer was considered instead to prevent the mixing of the molten Al and Mg alloys. Figure 15A shows the relationship between nugget size and welding current for welds made with the Zn-coated steel interlayer. It was noted that the nugget on the Mg side always was larger than that on the Al side,(Ref. 16). Tensile shear testing suggested stronger Mg/steel interface than Al/steel interface. As shown in Fig. 15B, welds made with a welding current of 28 kA and higher easily met the strength requirements of AWS D17.2.Figure 16 shows hardness distribution across a typical Al/Mg weld made with a Zn-coated steel interlayer. It can be observed that hardening did not occur either in the Mg or Al alloy fusion zones, which suggests that formation of a

ISSN (Online) 2456-1290
International Journal of Engineering Research in Mechanical and Civil Engineering (IJERMCE)
Vol 2, Issue 4, April 2017

large amount of brittle intermetallics was avoided and that negligible intermetallics were formed involving Zn due to the low quantity of this element originating from the coating.

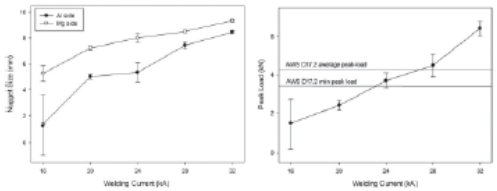

Fig. 15 — A - Correlation between nugget size on Al and Mg sides and welding current during RSW with a Zncoated steel interlayer. B - Correlation between peak load and welding current during RSW of Al to Mg with Zncoated steel interlayer.

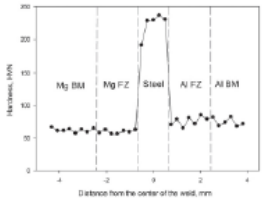

Fig. 16 — Hardness distribution across Al/Mg weld made with a Zn coated steel interlayer and 28kA welding current.

Al/Steel Interface Microstructure

Figure 17 shows an optical micrograph of a typical Al/Mg weld with a Zn-coated steel interlayer. It 8 showed more interfacial defects at the Al/steel interface than at the Mg/steel interface. The interface inside the fusion nugget was denoted as AS-I, the region adjacent to the nugget as AS-II, and the region where welding occurred through the Zn-rich phase, as zone AS-III. None of the Zn coating was found between the Al and steel anywhere in zone AS-I. Zinc was melted and squeezed from the nugget due to its low melting point (420°C). Microstructures of the interface at the center of the nugget exhibit a distinct Al-Fe reaction layer with an average thickness of 1.3mm.From Fig. 19, it was seen that voids were located close to the Al-Fe reaction layer. Almost no voids were observed at the edge of the nugget, while the Al- Fe reaction layer still was present. Overall, a reaction layer observed at the Al/steel interface (Fig. 19) should not severely deteriorate the strength of the joints since cracks were not observed, and the maximum thickness of intermetallics did not exceed 1.3 mm.

Fig. 17— Typical Al/Mg weld made with a Zn coated steel interlayer and 28kA welding current.

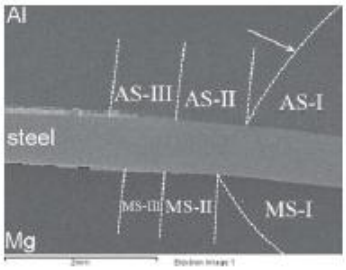

Fig. 18— Location of the zones that exhibit different interfacial microstructures in an Al/Mg weld made with a Zncoated steel interlayer and 28kA welding current.

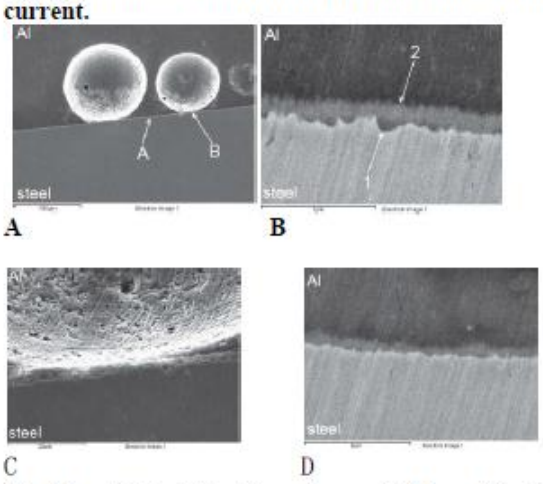

Fig. 19— Al/steel interface of zone ASI from Fig. 5: A — Center of ASI;B — details of A from A; C — details of B from A; D — zone ASI close to the boundary with ASII.

ISSN (Online) 2456-1290
International Journal of Engineering Research in Mechanical and Civil Engineering (IJERMCE)
Vol 2, Issue 4, April 2017

Fracture Morphology

Figure 20 shows regions of the fracture surface that correspond to the interfacial microstructure zones AS-I, AS-II, and AS-III (Fig. 18). It was seen from Fig. 20B that in the center of zone AS-I failure occurred inside the Al fusion zone close to the interface (region 7 in Fig. 20B). An Fe-Al intermetallic compound layer was found under the voids, and ductile fracture surfaces corresponding to the Al alloy fusion zone can be found between the voids (region 8 in Fig. 20B), which suggests that porosity decreased joint strength. Figure 20C shows the edge of the AS-I zone (region D in Fig. 20A). The fracture morphology of this region is similar to that of the center of zone AS-I, but smaller voids than in the center. A few river-like voids (region 9 in Fig. 20C) can be observed in the region as a result of accumulation of smaller voids (Ref. 17). Figure 20D shows the fracture morphology of zone AS-II, which was adjacent to the fusion nugget, and appears to be where solidstate welding between Al and steel occurred — Fig.19A. The surface morphology of the region suggests that fracture occurred either at the Al/steel interface (region 10 in Fig. 20D) or inside the Al sheet (region 11 in Fig. 20D). Figure 20E shows the fracture surface of zone AS-III where the Al-Zn reaction layer was observed at the Al/steel interface .Based on the fracture morphology and interfacial microstructure analysis (Fig. 20B), it can be concluded that welding in this region was promoted by the presence of Zn, which contributed to the strength.

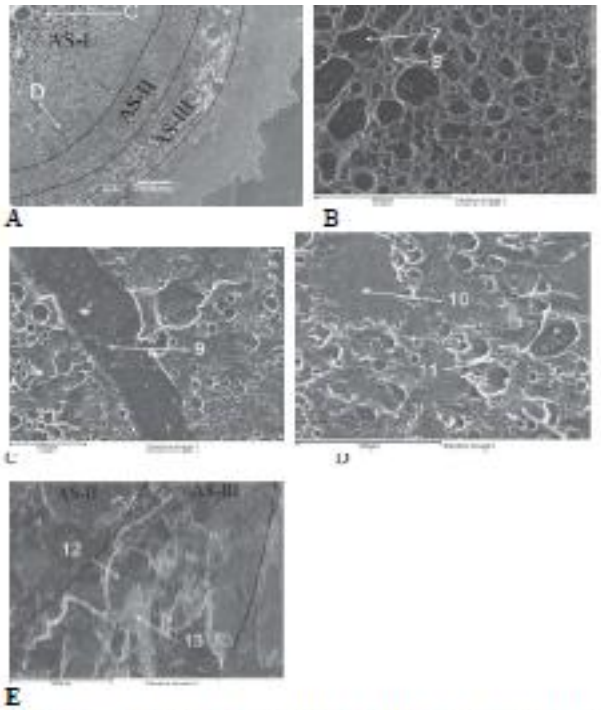

Fig. 20— Fracture surface of the Zn coated steel interlayer at Al side (produced in a weld made using 28 kA). A— Overview; B — details of region C from A; C — details of region D from A; D — details of zone ASII from A; E— details of zone ASII from A.

FATIGUE PERFORMANCE OF SPOT WELDS IN ADVANCED HIGH-STRENGTH STEELS

S. K. Vanimisetti And D. R. Sigler (5) undertook study to identify significant microstructural features that govern the fatigue life of spot welds and their relation to key process parameters to facilitate the optimization of the welding process for improving the fatigue performance of spot welded AHSS.

Experimental Procedure

Weld specimens, compositions and fatigue performance data from a previous study (Ref. 18) of spot-welded 1.6-mm galvannealed TRIP590 and 1.6-mm hot dip galvanized

ISSN (Online) 2456-1290
International Journal of Engineering Research in Mechanical and Civil Engineering (IJERMCE)
Vol 2, Issue 4, April 2017

(HDG) DP600 were chosen. Metallographic examination of weld cross-section was performed using optical microscopy. Microstructural parameters such as the nugget size, HAZ width, and FGHAZ orientation were measured from a high-resolution image of the microstructure using image analysis software, ImagePro® The angles between the extreme boundaries of the FGHAZ (inclined yellow lines), i.e., the CGHAZ-FGHAZ and FGHAZ-base material transition regions, and the faying interface (horizontal yellow line) were measured.

Modeling of Spot Weld Fatigue Failure

The fatigue performance of the weld is governed by the stress intensity factors and the crack propagation rates.The FE modeling method can also account for details such as weld indentation, crack growth, and notch root radius. In this study, the approach presented in Ref. 19 was adapted to study the change in stress intensity factor at the tip of a finitely long fatigue crack emanating from the notch root. A finite element (FE) model of the tensile lap-shear spot weld based on Ref. 19 was developed to estimate the stress intensity factors at the tip of a fatigue crack growing from the notch root, inclined at various angles with respect to the faying interface.

Modeling of Resistance Spot Welding

The computer simulation of the resistance spot welding process was carried out using commercial software SORPAS®.

Identification of Weld Micro-structural Zones from Simulations

The spatial maps of peak temperature (Tpk) and T85 cooling rate, i.e., the time taken for the sheet material to cool between 800° and 500°C during the welding process, were obtained from the simulations and were processed by visualization software, TECPLOT ® (Ref. 20).

Design of Experiments

Various parameters like joint design parameters (sheet material, stack configuration, etc.,), welding process parameters (schedule, electrode, etc.), and manufacturing variability (electrode misalignment, ambient, surface contamination, etc.) that influence the microstructure which in turn influences the fatigue performance of the joint were considered.

Spot Weld Microstructure and Fatigue Failure

Metallographic examination shows the fatigue crack has clearly grown from the faying interface through the FGHAZ to the outer surface of the sheet resulting in failure. An IPF map was generated from an EBSD analysis of the TRIP590 sample (see inset in Fig. 21B) in order to verify the observation from optical micrographs. Both optical micrographs and IPF maps consistently identified the spatial variation in the grain structure from the base material to the nugget. The high cycle fatigue failure is suggesting that a correlation might exist between FGHAZ orientation and fatigue life.

To verify this, more detailed measurements of the FGHAZ were carried out which indicated that samples with the lower FGHAZ angle of ~60 deg had shorter life, by almost an order of magnitude compared to samples with a higher FGHAZ angle of ~80 deg. Interestingly, the measurements also revealed that the FGHAZ angle in the galvanized DP600 material was consistently higher by ~8 deg than that in the galvannealed TRIP590 material.

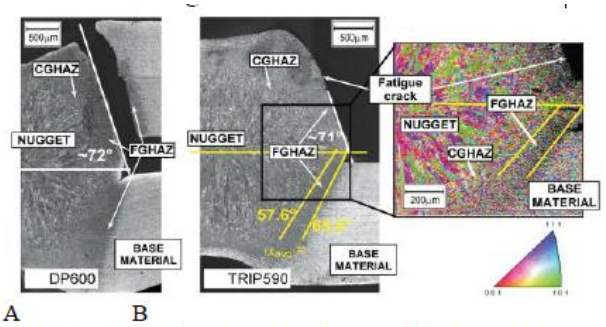

A B

Fig. 21 — Influence of microstructural zones on the fatigue crack growth in A — DP600; B — TRIP590 spot welds.

ISSN (Online) 2456-1290
International Journal of Engineering Research in Mechanical and Civil Engineering (IJERMCE)
Vol 2, Issue 4, April 2017

The profound effect of FGHAZ angle on fatigue life becomes apparent by plotting FGHAZ angle against cycles to failure as shown in Fig. 22. Samples with FGHAZ angle measurements are indicated by filled symbols, whereas those without are shown using hollow symbols. The FGHAZ angles were segregated into five distinct ranges, namely, very low angles (<65 deg), low angles (65–70 deg), medium angles (70–75 deg), high angles (75–80 deg), and very high angles (>80 deg). It is apparent from Fig. 5A, B that the FGHAZ angle correlates directly with fatigue life at all load levels, i.e., higher FGHAZ angles correlate with extended life. This effect is more pronounced for high cycle fatigue at 600-lb load, which shows almost an order of magnitude increase in the fatigue life as the FGHAZ orientation increases from low to high angles.

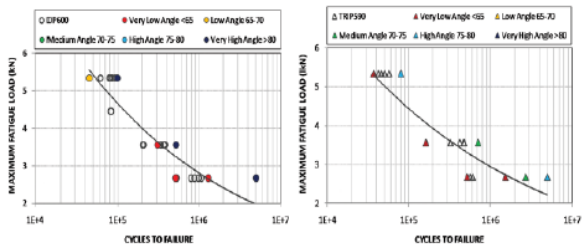

A B

Fig. 22 — Influence of FGHAZ angle on the fatigue performance of A — DP600; B — TRIP590 spot welds.

Influence of FGHAZ Orientation on High Cycle

Fatigue Crack Propagation

Fatigue crack growth occured along the FGHAZ, which provides a path for easier crack growth an angle of about 72 deg with reference to the faying interface. Finite element analyses were carried out to determine the stress intensity factors (SIFs) at the tip of fatigue cracks for cracks of various length of 1, 5, and 10% of the sheet thickness orientated at angle ‘’ with respect to the faying interface. The critical fatigue crack initiation and growth from points A and C along the loading symmetry plane occurs predominantly under mixed-mode I and II loading for which SIFs (KI and KII) at the crack tip were estimated using the finite element simulations. (Keq) was estimated using the following equation (Refs. 21–23)

$$K_{eq} = (K_I^2 + \beta K_{II}^2)^{1/2}$$

is a material parameter often close to 1.0. The fatigue crack initiation occurs in the direction o which can be written in as (Refs. 21-23).

$$\cos\theta_o = \frac{3\sin^2\Pi Me/2 + (\cos^4\Pi Me/2)^{1/2} + 8\cos^2\Pi Me/2 \sin^2\Pi Me/2}{\cos^2\Pi Me/2 + 9\sin^2\Pi Me/2}$$

From above Equation , it was seen that o ~ 0 deg for Me ~ 0, i.e., the crack will initiate and continue to grow in the direction where Me(Me = 2/ tan–1{KII/KI}) is minimized. The results of the finite element modeling study are presented in Fig. 23, which indicates preferred direction of fatigue crack propagation in lap-shear joints to be ~76 deg

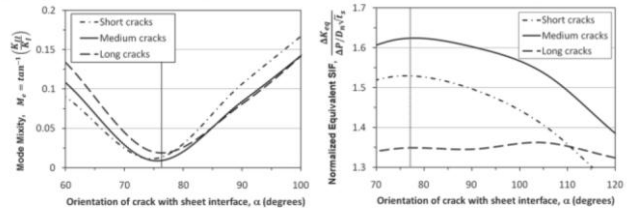

A B

Fig. 23— Effect of fatigue crack orientation on A — Mode mixity ; B — equivalent stress intensity factor .

WELD JOINT PROPERTIES

Triple Thin Sheet Aluminum Alloy Resistance Spot Welds

The microstructure in the three-sheet 6061 aluminum alloy RSWs consisted of a partially melted zone (PMZ), columnar grain zone (CGZ), and equiaxed grain zone

ISSN (Online) 2456-1290
International Journal of Engineering Research in Mechanical and Civil Engineering (IJERMCE)
Vol 2, Issue 4, April 2017

(EGZ), where the columnar grain zone is divided into the columnar grain with large secondary dendrite arm spacing (LCGZ) and the columnar grain with small secondary dendrite arm spacing (SCGZ). Three failure modes the interfacial (IF) failure, partial thickness-partial pull-out (PT-PP) failure, and pullout (PO) failure, were observed.

Constitutive Behavior of Dissimilar Aluminum Alloy Resistance Spot Welds

Three types of spot welds between dissimilar aluminum alloys, namely, Aural-2-T7 to Aural-2-T7, Aural- 2-T7 to AA5754- O, and Aural-2-T7 to AA6022-T4, were successfully produced using General Motors's proprietary MRD resistance spot welding process. All the weld nuggets were found to have higher yield strength than the base Aural-2-T7 material as a result of grain refinement during the resistance spot welding process and would be typical for any combination of Al alloy stack-ups containing at least one cast alloy because of the relatively fast solidification rates inherent in resistance spot welding..

Dissimilar resistance spot welds in AISI 430 ferritic stainless steel and DQSK low-carbon steels

Fusion zone was featured by dual phase micro-structure of ferrite and martensite controlled by austenite stability. The main metallurgical features in the HAZ of FSS side are grain growth and carbide precipitation whereas DQSK side was dictated by martensitic and eutectoid transformations. Increasing the welding current promoted double pullout mode.

Dissimilar Al/Mg joints produced by resistance spot welding with an interlayer

Poor strength joints were produced with a Zn foil interlayer due to formation of brittle intermetallic phases whereas Zn-coated steel interlayer gave much higher strength due to prevention of mixing of the Al and Mg alloys . The joint area on both Al and Mg sides could be divided into three regions from the center to the edge: weld brazing of molten metal, solid-state welding, and soldering of Al (or Mg) to steel via the Zn-rich filler metal.

Fatigue Performance of Spot Welds in Advanced High-Strength Steels

For AHSS, spatial orientation of the FGHAZ influenced the fatigue performance of the weld, especially high cycle fatigue. It was observed that FGHAZ that had high angles relative to the faying interface or were located well beyond the notch root improved fatigue performance due to retarded crack growth rates. This can be attributed to the crack growing at non-preferred angles with reduced

stress intensity and enhanced mixity or crack deflecting into the weld nugget where it encountered the hard nugget structure. The optimal electrode design showed a 23% increase in the FGHAZ angle (for a nominal nugget size of 5.5 mm) compared to a conventional weld electrode and multipulse schedule.

REFERENCES

1.Y. Li, Y. Zhang, Z. Luo, H. Shan, Y. Q. Feng, And Z. X. Ling. 2016. Failure Mode Transition Of Triple Thin Sheet Aluminum Alloy Resistance Spot Welds Under Tensile Shear Loads. Welding Journal 95(12): 479-S To 490-S.

2. J. Kang, B. Shalchi-Amirkhiz, Y. Chen, D. R. Sigler, And B. E. Carlson 2016.Characterization Of Constitutive Behavior Of Dissimilar Aluminum Alloy Resistance Spot Welds. Welding Journal 95(07): 248-S To 256-S.

3. M. Pouranvari, S. P. H. Marashi, And M. Alizadeh-Sh 2015. Welding Metallurgy Of Dissimilar Aisi 430/Dqsk Steels Resistance Spot Welds. Welding Journal 94(06): 203-S To 210-S.

4. P. Penner, L. Liu,A. Gerlich, And Y. Zhou. 2014. Dissimilar Resistance Spot Welding Of Aluminum To Magnesium With Zn-coated Steel Interlayers.Welding Journal 93(06): 225-S To 231-S

5. S. K. Vanimisetti And D. R. Sigler 2014. Improving Fatigue Performance Of Spot Welds In Advanced High-Strength Steels. Welding Journal 93(05): 153-S To 161-S.

6. Hongyan, Z., And Jacek, S. 2012. Resistance Welding: Fundamental And Applications, 2nd Ed. Boca Raton, Crc Press.

07. Drebushchak, V. A. 2008. The Peltier Effect. Journal Of Thermal Analysis And Calorimetry 91(1): 311–315.

08. Li, B. Q. 2002. Research on the numerical Simulation of the Process for Aluminum Alloy

Resistance Spot Welding and Energy Analysis. PhD Dissertation. Tianjin, Tianjin University .

09. Pouranvari, M., Marashi, S. P. H., and Mousavizadeh, S. M. 2010. Failure mode transition

and mechanical properties of similar and dissimilar resistance spot welds of DP600 and low carbon steels. Science and Technology of Welding and Joining 15(7): 625–631

10. Kang, J., McDermid, J. R., and Bruhis, M. 2013. Determination of the constitutive behavior of AA6022-T4 aluminum alloy spot welds at large strains. Materials Science and Engineering A A567: 95–100

11. Kaufman, J. G. 2000. Introduction to Alloys and Tempers, ASM International, Materials Park, Ohio.

12. Zhang, H., and Senkara, J. 2011. Resistance

Welding: Fundamentals and Applications, Second Edition, CRC Press.

13. North American Die Casting Association: High Integrity Die Castings. 2008. Arlington Heights, Ill.: North American Die Casting Association

14. Pouranvari, M., and Marashi, S. P. H. 2013. Critical review of automotive steels spot welding: process, structure and properties. Science Technology Welding Joining 18: 361–403.

15. Self, J. A., Olson, D. L., and Edwards, G. R. 1987. The stability of austenitic weld metal. NBS Publication on Cryogenic Properties of Metals: 181–189

16. Penner, P., Liu, L., Gerlich, A., and Zhou, Y. 2013. Feasibility study of resistance spot welding of dissimilar Al/Mg combinations with Ni based interlayers. Science and Technology of Welding & Joining 18(7): 541–550.

17. Tan, W., Zhou, Y., and Kerr, H. 2002. Effects

of Au plating on small-scale resistance spot welding of thin-sheet nickel. Metallurgical and Materials Transactions A 33(8): 2667—2676.

18. Sigler, D. R., and Vanimisetti, S. K. 2012.HAZ geometry in advanced high strength steel spot welds and its effect on fatigue performance. Proceedings AWS Sheet Metal Welding Conference XV, Livonia, Mich., Oct. 2–5.

19. Wang, D.-A., and Pan, J. 2005. A computational study of local stress intensity factor solutions for kinked cracks near spot welds in lap-shear specimens. Int. J. Solids Structures 42: 6277–6298.

20. Sigler, D. R., and Vanimisetti, S. K. 2012. HAZ geometry in advanced high strength steel spot welds and its effect on fatigue performance. Proceedings AWS Sheet Metal Welding Conference XV, Livonia, Mich., Oct. 2–5.

21. Radaj, D. 1990. Local fatigue strength characteristic values for spot welded joints. Engineering Fracture Mechanics 37(1): 245–250.

22. Biner, S. B. 2003. Fatigue crack growth studies under mixed-mode loading. Int. J. Fatigue 23: S259–S263.

23. Newman, J. A., and Dowling, N. E. 1998. A crack growth approach to life prediction spotwelded lap joints. Fatigue and Fracture of Engineering Materials & Structures 21: 1123–1132.